doi:10.1093/brain/awz072 BRAIN 2019: 142; 1195–1202 | 1195

BRAIN
A JOURNAL OF NEUROLOGY

REPORT

Absence of iron-responsive element-binding protein 2 causes a novel neurodegenerative syndrome

Gregory Costain,[1] Manik C. Ghosh,[2] Nunziata Maio,[2] Amanda Carnevale,[1] Yue C. Si,[3] Tracey A. Rouault[2] and Grace Yoon[1,4]

Disruption of cellular iron homeostasis can contribute to neurodegeneration. In mammals, two iron-regulatory proteins (IRPs) shape the expression of the iron metabolism proteome. Targeted deletion of *Ireb2* in a mouse model causes profoundly disordered iron metabolism, leading to functional iron deficiency, anemia, erythropoietic protoporphyria, and a neurodegenerative movement disorder. Using exome sequencing, we identified the first human with bi-allelic loss-of-function variants in the gene *IREB2* leading to an absence of IRP2. This 16-year-old male had neurological and haematological features that emulate those of *Ireb2* knockout mice, including neurodegeneration and a treatment-resistant choreoathetoid movement disorder. Cellular phenotyping at the RNA and protein level was performed using patient and control lymphoblastoid cell lines, and established experimental assays. Our studies revealed functional iron deficiency, altered post-transcriptional regulation of iron metabolism genes, and mitochondrial dysfunction, as observed in the mouse model. The patient's cellular abnormalities were reversed by lentiviral-mediated restoration of IRP2 expression. These results confirm that IRP2 is essential for regulation of iron metabolism in humans, and reveal a previously unrecognized subclass of neurodegenerative disease. Greater understanding of how the IRPs mediate cellular iron distribution may ultimately provide new insights into common and rare neurodegenerative processes, and could result in novel therapies.

1 Division of Clinical and Metabolic Genetics, Department of Paediatrics, The Hospital for Sick Children, University of Toronto, Toronto, Ontario, Canada
2 *Eunice Kennedy Shriver* National Institute of Child Health and Human Development, National Institutes of Health, Bethesda, Maryland, USA
3 GeneDx, Gaithersburg, MD, USA
4 Division of Neurology, Department of Paediatrics, The Hospital for Sick Children, University of Toronto, Toronto, Ontario, Canada

Correspondence to: Grace Yoon, MD, FRCP(C)
Division of Clinical and Metabolic Genetics, The Hospital for Sick Children
555 University Avenue, Toronto, Ontario M5G 1X8, Canada
E-mail: grace.yoon@utoronto.ca

Keywords: chorea; mitochondrial dysfunction; iron metabolism; neurodegeneration; *IREB2*

Abbreviations: IRE = iron-responsive element; IRP = iron-responsive element-binding protein

Received October 26, 2018. Revised January 7, 2019. Accepted January 31, 2019. Advance Access publication March 26, 2019

Introduction

Altered distribution of cellular iron may contribute to the pathogenesis of both common and rare neurodegenerative conditions, such as Alzheimer's disease, Parkinson's disease, Friedreich ataxia, Huntington's disease, and the neurodegeneration with brain iron accumulation disorders (LaVaute *et al.*, 2001; Cooperman *et al.*, 2005). The molecular mechanisms that regulate iron metabolism in humans are incompletely understood. Intracellular iron homeostasis in mammals is maintained by two ubiquitously expressed iron-responsive element-binding proteins (IRPs) (Rouault, 2013; Ward *et al.*, 2014). IRP1 and IRP2 post-transcriptionally regulate the expression of transferrin receptor 1 (TFRC), heavy and light chain ferritin (FTH and FTL), and other proteins involved in iron metabolism and oxygen sensing, by binding to iron-responsive elements (IREs) in their messenger RNAs (Fig. 1). IRP1 is a bifunctional protein that binds to IREs in iron-deficient conditions when it is an apoprotein, but it converts to cytosolic aconitase in iron-replete conditions upon acquisition of a [4Fe-4S] cluster. IRP2 is homologous to IRP1 but undergoes iron-dependent degradation in iron-replete cells.

The consequences of disrupting the IRE-IRP system in humans have not been described previously. However, mice with targeted deletion of *Ireb2* overexpress ferritin, and have abnormally low TFRC levels and high ferritin levels in multiple tissues (Ghosh *et al.*, 2015). Despite this misregulation, we have not detected pathological consequences in tissues such as liver and kidney, where Irp1 is highly expressed and is able to fully compensate for the loss of Irp2. The CNS and erythropoietic systems are particularly affected in the *Ireb2*-knockout mice, where evidence of abnormal iron metabolism precedes the development of adult-onset progressive neurodegeneration characterized by widespread axonal degeneration and neuronal loss associated with increased iron accumulation in axonal structures and oligodendrocytes (LaVaute *et al.*, 2001; Cooperman *et al.*, 2005). Therefore, targeted disruption of *Ireb2* in mice results in mild anaemia, erythropoietic protoporphyria, and a neurodegenerative movement disorder (Supplementary Video 1).

We describe here the first patient with bi-allelic loss-of-function variants in *IREB2* leading to complete absence of IRP2 protein. The clinical and cellular phenotypes of this severely impaired 16-year-old male recapitulate the

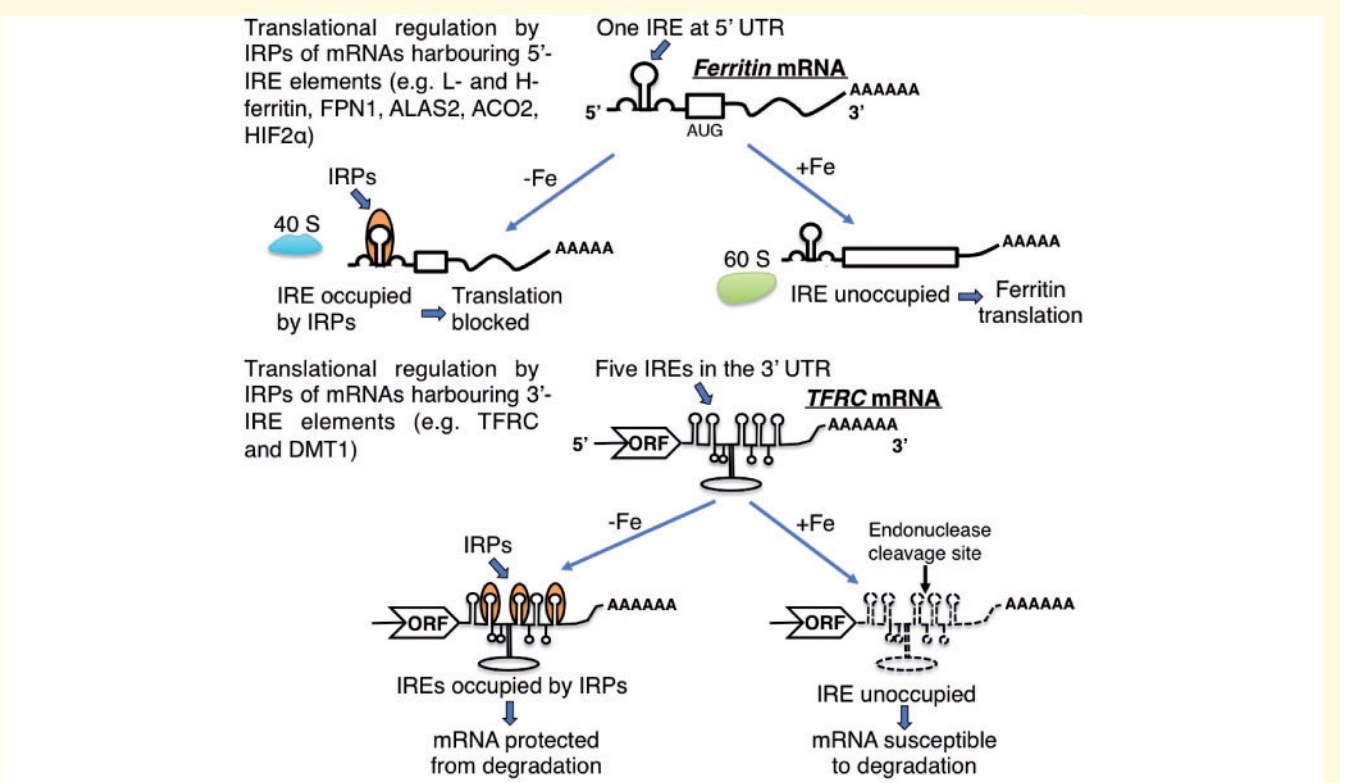

Figure 1 Schematic representation of the mechanism of cellular iron sensing mediated by the IRE-IRP system. In iron-deficient cells (−Fe), iron regulatory proteins 1 and 2 (IRPs) enhance iron uptake and decrease iron sequestration by binding to iron-responsive elements (IREs) present at the 5′-UTRs of transcripts like the iron storage protein ferritin, blocking their translation, and at the 3′-UTRs of mRNAs such as transferrin receptor (*TFRC*), responsible for iron uptake, where binding confers protection against endonucleolytic cleavage. Conversely, under iron-replete conditions (+Fe), IREs remain unoccupied, iron uptake is reduced, and storage is promoted.

neurological and hematologic abnormalities that adversely affect *Ireb2*$^{-/-}$ mice (LaVaute *et al.*, 2001; Cooperman *et al.*, 2005). These findings represent the confirmation of predictions that complete loss of IRP2 would cause human pathophysiology, including neurodegenerative disease.

Materials and methods

Patient recruitment and genotyping

The patient has received care at our hospital since infancy, and was followed over the past 7 years in a specialized Neurogenetics Clinic at The Hospital for Sick Children (Toronto, Canada). Extensive genetic and non-genetic investigations were initially non-diagnostic (Supplementary material), prior to the decision to pursue whole exome sequencing. Using genomic DNA from the proband and parents, the exonic regions and flanking splice junctions of the genome were captured using the Clinical Research Exome kit (Agilent Technologies). Massively parallel (NextGen) sequencing was carried out on an Illumina system with 100 bp or greater paired-end reads. Reads were aligned to human genome build GRCh37/UCSC hg19, and analysed for sequence variants using a custom-developed analysis tool. The sequencing and variant interpretation protocols have been previously described in detail (Retterer *et al.*, 2016). The general assertion criteria for variant classification are publicly available on the GeneDx ClinVar submission page (http://www.ncbi.nlm.nih.gov/clinvar/submitters/26957/).

Experimental methods

The full methods are presented in the Supplementary material. Immortalized lymphoblastoid cell lines for the proband and his father were generated at The Centre for Applied Genomics (Toronto, Canada). The latter were used as a control. Patient derived lymphoblasts, which completely lacked IRP2 protein, were subsequently engineered to stably express human *IREB2*. Neomycin resistant clones were isolated, analyzed for IRP2 expression by western blot, and expanded and used in all the experiments presented in this study. RNA was isolated using the RNeasy® kit from QIAGEN. Reverse-transcription was performed on total RNA using SuperScript™ III (Invitrogen) and random hexamers. Real-time PCR on complementary DNA was performed with SYBR® Green PCR Master Mix (Applied Biosystems) on an ABI 7000. Relative transcript abundance was calculated using the $2^{-\Delta\Delta Ct}$ method, with *Actb* as the internal control. Cellular fractionation into cytosol and intact mitochondria was carried out as described previously (Frezza *et al.*, 2007; Maio *et al.*, 2014). The NativePAGE Novex Bis-Tris gel system (Thermo Fisher Scientific) was used for the analysis of mitochondrial respiratory complexes, and in-gel complex I, II and IV activity assays were performed as described previously (Maio *et al.*, 2014). Labile iron pool measurements were performed as previously described (Kakhlon and Cabantchik, 2002). Iron concentrations in the patient and control lymphoblast cells were determined by inductively coupled plasma mass spectrometry (Agilent model 7900). Antibodies used in this study are described in the Supplementary material. Aconitase activity and gel retardation assays were performed as described previously (Meyron-Holtz *et al.*, 2004; Tong and Rouault, 2006).

Statistical analysis

Where applicable, data are expressed as the mean ± standard deviation. Pairwise comparisons between two groups were performed using the unpaired Student's *t*-test. Analyses of multiple groups were performed using two-way ANOVA. *P*-values of <0.05 were considered statistically significant.

Data availability

Data presented in this study are available upon reasonable request.

Ethics statement

This study was approved by the Research Ethics Board of The Hospital for Sick Children. The parents provided written informed consent to participate in this study, including publication of photographs and videos.

Results

Clinical summary

The 16-year-old male patient was born to healthy non-consanguineous parents of Filipino descent following a normal pregnancy and delivery at full-term. Poor head control with significant axial hypotonia was identified at 3 months. The patient developed intermittent dystonic posturing shortly thereafter. He was diagnosed after 1 year of age with dystonic cerebral palsy (Gross Motor Function Classification System level V). He demonstrated profound early global developmental delays, and was never able to ambulate or speak. In childhood he developed a choreoathetoid movement disorder, characterized by upper extremity chorea and oromotor dyskinesias. A trial of trihexyphenidyl was not successful. Lower extremity hypertonia and spasticity emerged over time. He developed generalized tonic-clonic seizures at 9 years. EEG had consistently shown diffuse background slowing, a lack of posterior rhythm and sleep architecture, and frequent focal epileptiform activity. At age 16 years, good seizure control was achieved using the antiepileptic drugs oxcarbazepine and clobazam.

At the time of last assessment at age 16 years, he was non-ambulatory and could not roll or crawl. He had a fisted grasp and sometimes reached for objects placed in front of him, but did not transfer objects from one hand to the other or manifest a hand preference. There was paucity of voluntary movements, but he had prominent choreiform movements of the face, buccal-oral-lingual region, trunk, and upper limbs (Supplementary Video 2). There were no abnormal eye movements. There was minimal facial recognition and minimal eye contact. He had corticospinal tract signs with severe hypertonia, hyperreflexia and bilateral extensor plantar response. He was non-

verbal and emitted occasional babbling noises and vowel sounds. He was dependent for all aspects of self-care and required a gastrostomy tube for nutrition.

Brain MRI at 12 and at 18 months showed prominent extra-axial CSF spaces suggestive of cerebral volume loss, prominent ventricles, mildly delayed myelin maturation, and moderate loss of white matter volume that appeared most marked in the frontal regions (Fig. 2A and B). Brain MRI at 12 years showed mild prominence of the cerebellar interfoliate fissures and progression of cerebral atrophy and white matter volume loss (Fig. 2C and D). Single voxel magnetic resonance spectroscopy of the left basal ganglia identified a decreased *N*-acetylaspartate:choline ratio. Nerve conduction studies and electromyography at 12 years were normal. A dilated retinal examination was within normal limits, but electroretinography revealed evidence of retinal dysfunction.

He has also had longstanding microcytic hypochromic anaemia unresponsive to iron supplementation. At 15 years, his haemoglobin was 11.4 g/dl, mean corpuscular volume was 65.5 fl, serum ferritin was mildly elevated at 225.5 µg/l, and zinc protoporphyrin was markedly elevated at 352.0 µmol/mol Hgb (reference range 30.0–80.0 umol/mol Hgb), whereas his serum transferrin and iron levels were normal.

Molecular and cellular studies

Clinical exome sequencing revealed that the patient was a compound heterozygote for predicted loss-of-function variants in *IREB2* (GenBank: NM_004136.2; c.[1069G>T, p.G357X];[1255C>T, p.R419X]), the gene that encodes IRP2. IRP2 protein was undetectable, FTH was upregulated, and TFRC was downregulated in western blots performed on patient lymphoblast extracts (Fig. 3A and Supplementary Fig. 1A, C and D), as observed previously in multiple tissues in the murine model (LaVaute *et al.*, 2001). IRP1 protein levels and the IRE-binding

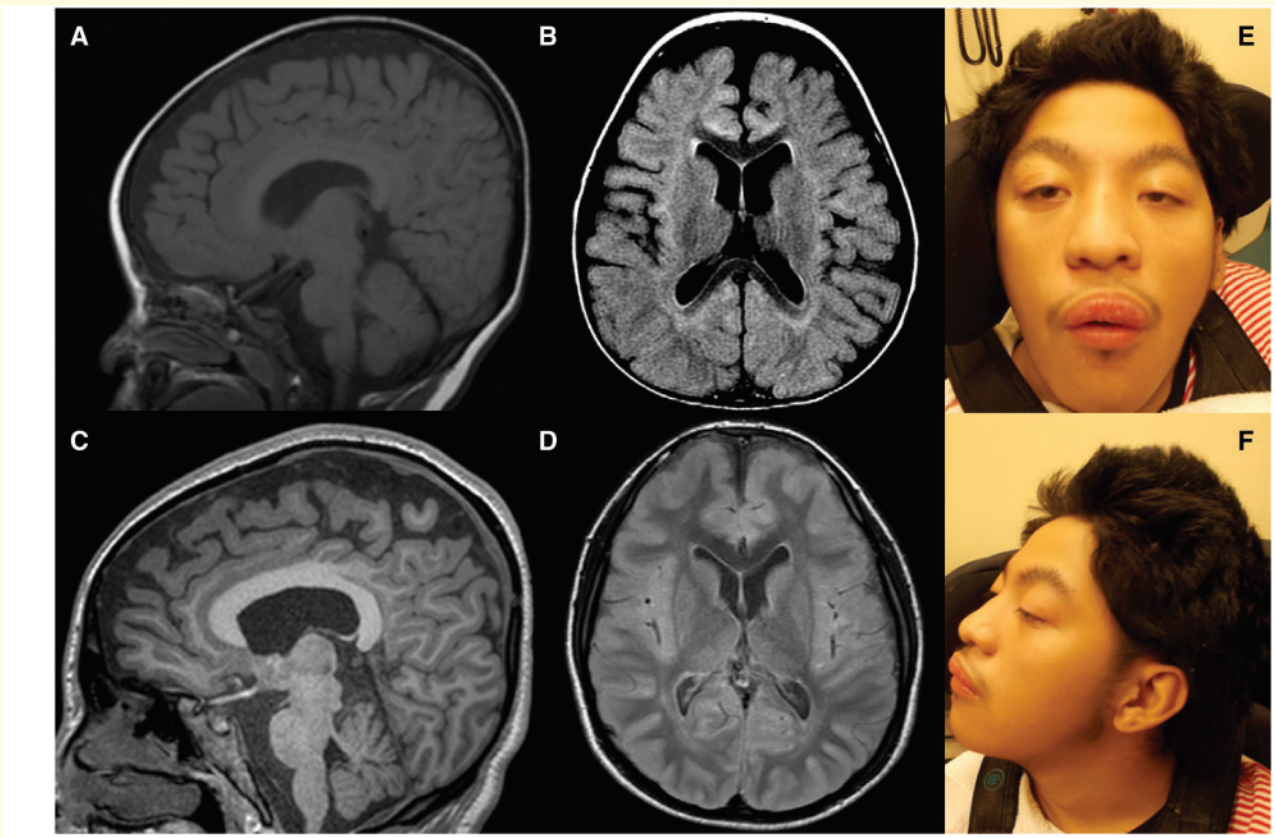

Figure 2 Selected brain MRI images and clinical photographs of an individual with bi-allelic loss-of-function variants in *IREB2*. Selected images from serial brain imaging of the patient (**A**–**D**). Sagittal T_1-weighted MRI (**A**) demonstrates prominent extra-axial CSF spaces suggestive of cerebral volume loss in the patient at age 18 months. The brainstem and posterior fossa structures are normal. Axial FLAIR (**B**) MRI obtained at the same time demonstrates prominent ventricles and mildly delayed myelin maturation, with moderate loss of white matter volume that appears most marked in the frontal regions. Matching subsequent T_1-weighted and FLAIR MRI at age 12 years reveals (**C**) mild prominence of the cerebellar interfoliate fissures and (**D**) progression of cerebral atrophy and white matter volume loss. Portrait and side profile photographs (**E** and **F**) taken at age 16 years 11 months demonstrate ptosis and mild non-specific facial dysmorphisms, including a short philtrum, low-set ears, and subtle midface hypoplasia. The scalp hair and body hair (not pictured) was thick, unruly, and wiry in texture, and differed from the hair of either parent (see also the fur of mice in Supplementary Video 1).

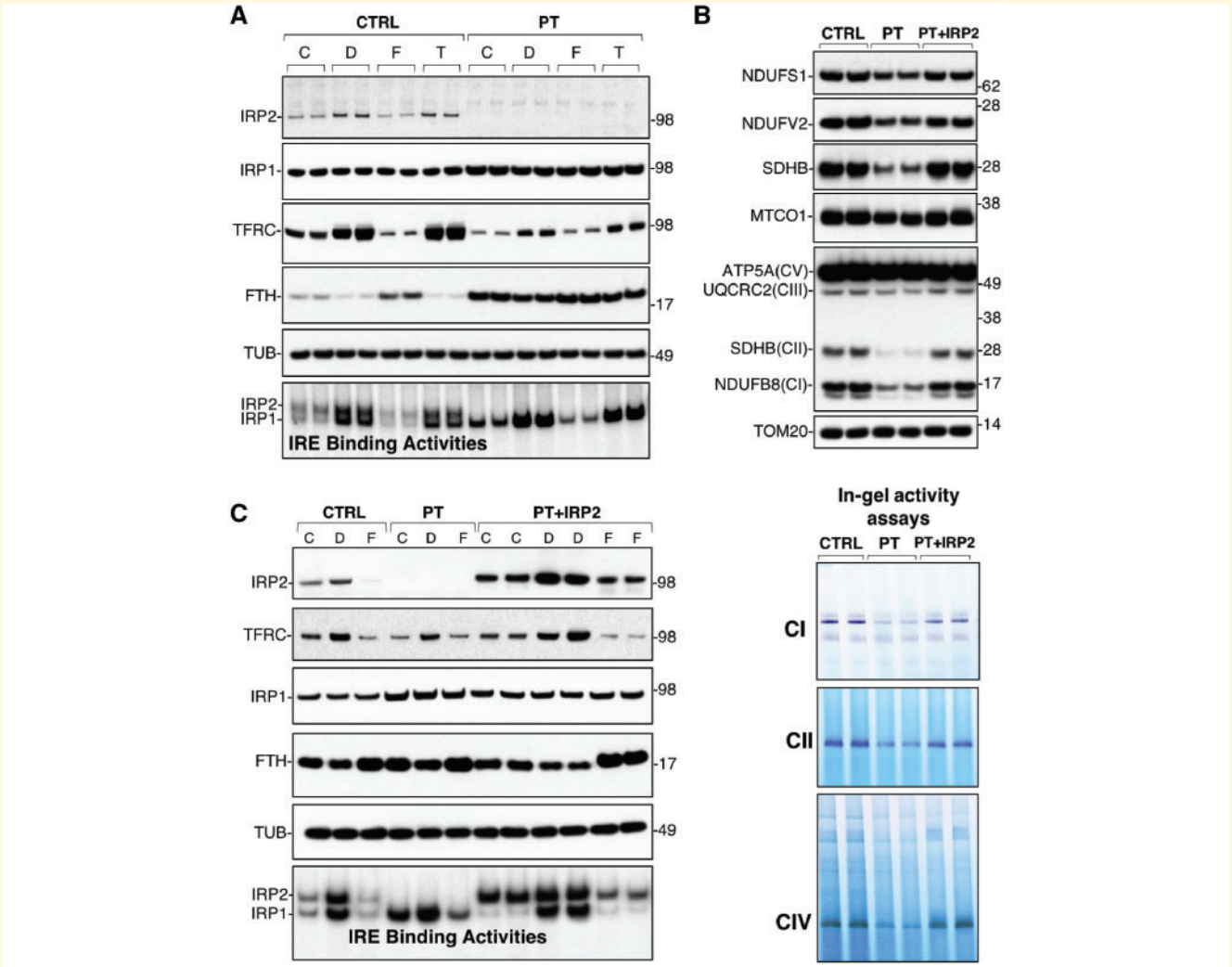

Figure 3 Complete loss of IRP2 in patient-derived lymphoblasts caused altered post-transcriptional regulation of iron metabolism genes and mitochondrial dysfunction. (**A**) Control (CTRL; obtained from the patient's father, who carries one normal allele and a G357X allele) and patient (PT) lymphoblasts grown for 16 h in unsupplemented medium (lanes C), medium supplemented with 100 μM of the iron chelator deferoxamine mesilate (lanes D), with 300 μM ferric ammonium citrate (lanes F), or with 300 μM of the stable nitroxide molecule Tempol (lanes T) were analyzed by western blot or gel-shift assay. Immunoblots and gel-shift assay confirmed the absence of IRP2 protein in the patient cells and showed significant downregulation of transferrin receptor and upregulation of H-ferritin (FTH), even though IRP1 protein levels increased ~2-fold in the patient cells. As expected, IRE-binding activities of IRP1 and IRP2 were increased in iron-depleted cells (lanes D) or in cells treated with Tempol, which shifted the equilibrium of IRP1 from the iron-sulfur cluster-containing cytosolic aconitase towards the IRE-binding apoform. Conversely, IRE-binding activities of IRP1 and IRP2 were decreased under iron-replete conditions (lanes F). (**B**) Immunoblots to NDUFS1 and NDUFV2 (complex I iron-sulfur subunits), SDHB (complex II iron-sulfur subunit), MTCO1 (complex IV subunit) and total OXPHOS showed decreased levels of subunits of the respiratory complexes in PT cells. Consistent with loss of constituent subunits, in-gel activity assays showed significantly decreased complexes I, II, and IV activities in the patient cells. Levels of subunits of respiratory complexes as well as activities were restored by re-expression of IRP2 in the patient cells. For quantification and statistical analysis, see Supplementary Fig. 1. (**C**) The altered phenotype of the patient cells was rescued by lentiviral-mediated transduction of IRP2 (PT + IRP2). TFRC protein levels were increased to levels comparable to CTRL and FTH levels were conversely effectively repressed under iron deficient conditions (lanes D). Gel shift assay confirmed restoration of IRP2 IRE-binding activity in the patient cells transduced with wild type IRP2 (PT + IRP2).

activity of IRP1 were increased ~2-fold in the patient cells, consistent with partial biological compensation for the loss of IRP2 (Fig. 3A and Supplementary Fig. 1B). Activities of cytosolic aconitase, respiratory chain complexes I, II, and IV, and protein levels of NDUFS1 and NDUFV2 (complex I iron-sulfur subunits), SDHB (complex II iron-sulfur subunit), and MTCO1 (complex IV subunit) were decreased in extracts from IRP2 null patient cells (Figs 3C, 4F and Supplementary Fig. 1I–O). The labile pool of accessible iron was decreased in the patient cells (Fig. 4H), although total cellular iron levels were unchanged (total cellular iron content, as assessed by inductively coupled

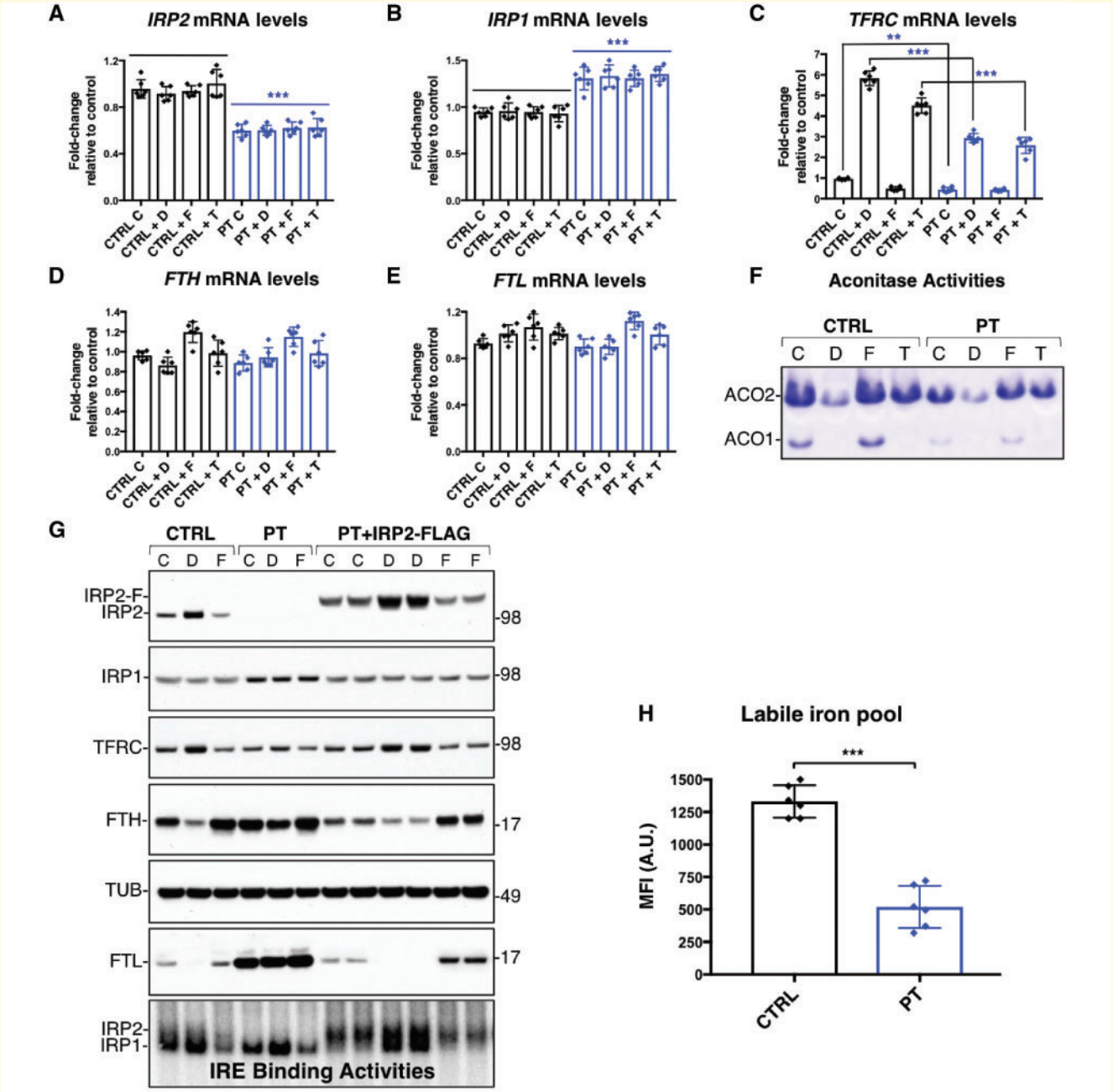

Figure 4 Biochemical characterization of IRP2-patient derived lymphoblasts. (**A**–**E**) mRNA levels of *IRP2*, *IRP1*, *TFRC*, H-ferritin (*FTH1*) and L-ferritin (*FTL*) in control and patient-derived lymphoblasts grown for 16 h in unsupplemented medium (lanes C), or in medium supplemented with deferoxamine mesilate (lanes D), ferric ammonium citrate (lanes F), or Tempol (lanes T). (**A**) *IRP2* mRNA levels were significantly lower in the patient cells compared to control (CTRL versus PT, $P < 0.0001$). (**B**) *IRP1* mRNA levels were significantly higher in the patient cells (CTRL versus PT, $P < 0.0001$). (**C**) *TFRC* mRNA levels were lower in the patient cells compared to control (CTRL C versus PT C, $P = 0.0031$; CTRL + D versus PT + D, $P < 0.0001$; CTRL + F versus PT + F, non significant; CTRL + T versus PT + T, $P < 0.0001$). (**F**) In-gel aconitase activity assay in control and patient lymphoblasts showed decreased cytosolic aconitase activity (ACO1) in the patient cells, consistent with abnormally elevated IRE-binding activity of IRP1 (Figs 3A, B and 4G) in the patient cells lacking IRP2. (**G**) The altered phenotype of the IRP2-patient cells was rescued by lentiviral-mediated transduction of C-terminally FLAG-tagged IRP2 (PT + IRP2-FLAG). TFRC protein levels were increased to levels comparable to CTRL and FTH and FTL levels were conversely effectively repressed under iron deficient conditions (lanes D). Gel shift assay confirmed restoration of IRP2 IRE-binding activity in the patient cells transduced with wild type recombinant IRP2-FLAG (PT + IRP2-FLAG). (**H**) Labile iron pool (LIP) measurements showed a significant reduction (≅2.6 fold) in the patient cells compared to control (CTRL versus PT, $P < 0.0001$), without significant changes in total cellular iron content, as assessed by inductively coupled plasma mass spectrometry (ICPMS). Total cellular iron content in control cells was 25.43 ± 2.56 ng of iron per 10^9 cells. Total cellular iron content in IREB2-deficient patient cells was 28.74 ± 1.63 ng of iron per 10^9 cells. Results in **A**–**E** and **H** are reported as mean ± SD. For quantification and statistical analysis of immunoblots in **G**, see Supplementary Fig. 2.

plasma mass spectrometry (ICPMS), in control cells was 25.43 ± 2.56 ng of iron per 10^9 cells and total cellular iron content in IREB2-deficient patient cells was 28.74 ± 1.63 ng of iron per 10^9 cells). These results suggest that functional iron deficiency developed in patient cells because of reduced iron uptake through TFRC, concomitant with markedly increased sequestration of iron within ferritin heteropolymers assembled from FTH and FTL subunits. All these abnormalities of the patient cells were reversed by lentiviral-mediated restoration of IRP2 expression (Figs 3B, C and 4G, and Supplementary Figs 1E–H and 2A–E).

Discussion

Our findings implicate bi-allelic loss-of-function variants in *IREB2* as the cause of a new human disease characterized by severe neurological and extra-neurological features. The patient's clinical and cellular phenotypes, including altered post-transcriptional regulation of iron metabolism genes and mitochondrial dysfunction, are remarkably concordant with those of the first knockout mouse model initially described in 2001 (LaVaute *et al.*, 2001; Cooperman *et al.*, 2005). Lentiviral-mediated restoration of IRP2 expression rescued the abnormalities observed in the lymphoblast cells of this patient, which provides further evidence for a causal association.

The existence of an autosomal recessive *IREB2*-related disorder has been hypothesized for several years (Ghosh *et al.*, 2015). Once identified, deep phenotyping of an individual with constitutional absence of IRP2 promised to address longstanding questions about the importance and internal redundancy of the IRP-IRE system in humans. This first report comes after nearly a decade of massive population-scale genome-wide sequencing efforts and the increasingly widespread use of exome sequencing in individuals with complex neurological disorders. Extensive efforts by our group to identify a second similarly affected individual were unsuccessful. The apparent rarity of *IREB2*-related disorders could reflect a strong negative selective pressure. Crosses of heterozygous *Ireb2*$^{+/-}$ mice resulted in a lower (15% of 300 offspring) than expected (25%) number of liveborn *Ireb2*$^{-/-}$ pups (Rouault laboratory, unpublished data). In humans, there are no homozygotes with loss-of-function variants in *IREB2* in large databases of genetic variation including the Genome Aggregation Database (gnomad.broadinstitute.org/; accessed January 2019) (Lek *et al.*, 2016). Although no severe phenotype was appreciated in our patient's healthy heterozygous carrier parents, findings from the Genome Aggregation Database indicate an extreme intolerance of *IREB2* to even mono-allelic loss-of-function variants, with nearly 10-fold fewer observed variants than expected (Lek *et al.*, 2016). As exome sequencing is used more frequently as a diagnostic tool in neurology, we anticipate more *IREB2*$^{-/-}$ patients will likely be identified, particularly in relatively inbred populations in which a founder mutation is present. Additionally, patients with missense mutations causing partial loss or gain of function of *IREB2* may prove to have more subtle clinical manifestations.

After the publication of the first *Ireb2* knockout mouse model (LaVaute *et al.*, 2001), two groups independently created additional models using different strains and methods (Galy *et al.*, 2006; Zumbrennen-Bullough *et al.*, 2014). These other mouse models of Irp2 deficiency demonstrated microcytic anemia, but their neurological deficits were thought to be subtle, as reviewed in detail elsewhere (Ghosh *et al.*, 2015). In particular, different conclusions were reached about CNS iron deposition and neurodegeneration in *Ireb2*$^{-/-}$ mice (Galy *et al.*, 2006; Ghosh *et al.*, 2015). This underscored the importance of assessing the physiological significance of loss of IRP2 directly in humans. The findings in our patient provide valuable confirmatory evidence that IRP2 is essential for mammalian iron metabolism in general, and for maintenance of CNS integrity in particular. Future considerations beyond the scope of the current study include creation of induced pluripotent stem cell derived neurons for further analyses.

Our results support the generalizability of a large body of basic experimental work on a mouse model (Rouault, 2013; Ghosh *et al.*, 2015). There is the potential for clinical translation of therapeutics shown to be beneficial in the knockout mice. For example, dietary supplementation with a stable nitroxide (Tempol) slowed progression of the underlying neurodegeneration in a mouse model (Ghosh *et al.*, 2008). Although Tempol is usually known to act as an antioxidant, in this context it functions as a mild oxidant on the [4Fe-4S] cluster of IRP1 to activate latent IRE-binding activity, thereby partially compensating for the loss of IRP2 (Ghosh *et al.*, 2008). The mitochondrial dysfunction observed in our patient and in the murine models also suggests a possible role for antioxidant therapies, as well as for avoiding medications with known mitochondrial toxicity, such as valproic acid. In the setting of functional iron deficiency, iron scavengers and chelation would not be considered as a treatment modality, however. This potentially contrasts with other neurogenerative disorders with brain iron accumulation where systemic iron status is typically unaffected (Ward *et al.*, 2014). Specific aspects of our patient's phenotype, such as his hyperkinetic movement disorder, are reminiscent of disorders such as Huntington's disease which also manifest abnormalities of cerebral iron metabolism (Muller and Leavitt, 2014; Sanchez-Castaneda *et al.*, 2015; Dietrich *et al.*, 2017), raising the possibility that established and emerging symptom-specific treatments may cross diagnostic boundaries. Understanding how the IRE-IRP system mediates cellular iron distribution might ultimately provide new insights into common and rare neurogenerative processes, and could result in novel therapies.

Acknowledgements

We would like to thank the family for their participation in this study; this work would not have been possible without their generosity.

Funding

This study was supported in part by the Intramural Program of the *Eunice Kennedy Shriver* National Institute of Child Health and Human Development.

Competing interests

The authors report no competing interests. Y.S. is an employee of GeneDx, Inc., a wholly owned subsidiary of OPKO Health, Inc.

Supplementary material

Supplementary material is available at *Brain* online.

References

Cooperman, SS, Meyron-Holtz, EG, Olivierre-Wilson, H, Ghosh, MC, McConnell, JP, Rouault, TA. Microcytic anemia, erythropoietic protoporphyria, and neurodegeneration in mice with targeted deletion of iron-regulatory protein 2. Blood 2005; 106: 1084–91.

Dietrich, P, Johnson, IM, Alli, S, Dragatsis, I. Elimination of huntingtin in the adult mouse leads to progressive behavioral deficits, bilateral thalamic calcification, and altered brain iron homeostasis. PLoS Genet 2017; 13: e1006846.

Frezza, C, Cipolat, S, Scorrano, L. Organelle isolation: functional mitochondria from mouse liver, muscle and cultured fibroblasts. Nat Protoc 2007; 2: 287–95.

Galy, B, Holter, SM, Klopstock, T, Ferring, D, Becker, L, Kaden, S, et al. Iron homeostasis in the brain: complete iron regulatory protein 2 deficiency without symptomatic neurodegeneration in the mouse. Nat Genet 2006; 38: 967–9; discussion 9–70.

Ghosh, MC, Tong, WH, Zhang, D, Ollivierre-Wilson, H, Singh, A, Krishna, MC, et al. Tempol-mediated activation of latent iron regulatory protein activity prevents symptoms of neurodegenerative disease in IRP2 knockout mice. Proc Natl Acad Sci USA 2008; 105: 12028–33.

Ghosh, MC, Zhang, DL, Rouault, TA. Iron misregulation and neurodegenerative disease in mouse models that lack iron regulatory proteins. Neurobiol Dis 2015; 81: 66–75.

Kakhlon, O, Cabantchik, ZI. The labile iron pool: characterization, measurement, and participation in cellular processes(1). Free Radic Biol Med 2002; 33: 1037–46.

LaVaute, T, Smith, S, Cooperman, S, Iwai, K, Land, W, Meyron-Holtz, E, et al. Targeted deletion of the gene encoding iron regulatory protein-2 causes misregulation of iron metabolism and neurodegenerative disease in mice. Nat Genet 2001; 27: 209–14.

Lek, M, Karczewski, KJ, Minikel, EV, Samocha, KE, Banks, E, Fennell, T, et al. Analysis of protein-coding genetic variation in 60,706 humans. Nature 2016; 536: 285–91.

Maio, N, Singh, A, Uhrigshardt, H, Saxena, N, Tong, WH, Rouault, TA. Cochaperone binding to LYR motifs confers specificity of iron sulfur cluster delivery. Cell Metab 2014; 19: 445–57.

Meyron-Holtz, EG, Ghosh, MC, Iwai, K, LaVaute, T, Brazzolotto, X, Berger, UV, et al. Genetic ablations of iron regulatory proteins 1 and 2 reveal why iron regulatory protein 2 dominates iron homeostasis. EMBO J 2004; 23: 386–95.

Muller, M, Leavitt, BR. Iron dysregulation in Huntington's disease. J Neurochem 2014; 130: 328–50.

Retterer, K, Juusola, J, Cho, MT, Vitazka, P, Millan, F, Gibellini, F, et al. Clinical application of whole-exome sequencing across clinical indications. Genet Med 2016; 18: 696–704.

Rouault, TA. Iron metabolism in the CNS: implications for neurodegenerative diseases. Nat Rev Neurosci 2013; 14: 551–64.

Sanchez-Castaneda, C, Squitieri, F, Di Paola, M, Dayan, M, Petrollini, M, Sabatini, U. The role of iron in gray matter degeneration in Huntington's disease: a magnetic resonance imaging study. Hum Brain Mapp 2015; 36: 50–66.

Tong, WH, Rouault, TA. Functions of mitochondrial ISCU and cytosolic ISCU in mammalian iron-sulfur cluster biogenesis and iron homeostasis. Cell Metab 2006; 3: 199–210.

Ward, RJ, Zucca, FA, Duyn, JH, Crichton, RR, Zecca, L. The role of iron in brain ageing and neurodegenerative disorders. Lancet Neurol 2014; 13: 1045–60.

Zumbrennen-Bullough, KB, Becker, L, Garrett, L, Holter, SM, Calzada-Wack, J, Mossbrugger, I, et al. Abnormal brain iron metabolism in Irp2 deficient mice is associated with mild neurological and behavioral impairments. PLoS One 2014; 9: e98072.